Gyrokinetic Studies of Nonlocal Properties of Turbulence-driven and Neoclassical Transport

W. X. Wang, T. S. Hahm, G. Rewoldt, J. Manickam, and W. M. Tang

Princeton Plasma Physics Laboratory, P.O. Box 451, Princeton, NJ 08543, USA

e-mail contact of main author: wwang@pppl.gov

Abstract. The nonlocal physics associated with turbulent and neoclassical transport is investigated using newly developed simulation capabilities and analytic models. For turbulence transport, we focus our studies on the turbulence spreading through a transport barrier characterized by an $\mathbf{E} \times \mathbf{B}$ shear layer. We perform a series of numerical experiments by placing a radial electric field well, with varying strength, next to the region where the ITG instability is linearly unstable. It is found that an $\mathbf{E} \times \mathbf{B}$ shear layer with an experimentally relevant level of the shearing rate can significantly reduce turbulence spreading by reducing the spreading extent and speed. From the spatio-temporal evolution of the turbulence propagation front, we find that the spreading slows down significantly in the region of higher shearing rate, rather than at the bottom of the E_r well. Our global neoclassical particle simulation using GTC-Neo, which includes nonlocal physics due to large orbit effects, studies neoclassical physics of NSTX plasmas. Typically, near the magnetic axis, the ion heat flux is decoupled from the local temperature gradient, breaking the Fick's law type gradient-flux relation. Our simulation predicts an outward ion heat flux, even for a reversed local ∇T_i near the magnetic axis, which is in the same direction as the experimental measurement.

1. Introduction

In this work, the nonlocal physics associated with turbulent and neoclassical transport is investigated using newly developed simulation capabilities[1] and analytic models. Our global gyrokinetic particle simulation incorporates important realism of tokamak experiments, including the comprehensive influence of non-circular cross section, realistic plasma profiles, plasma rotation, neoclassical (equilibrium) electric fields, Coulomb collisions, and other features. It has been interfaced with TRANSP, a widely used experimental data analysis software tool. It directly reads plasma profiles of temperature, density and toroidal angular velocity from the TRANSP experimental database, and numerical MHD equilibria reconstructed by the JSOLVER or ESC codes using TRANSP radial profiles of the total pressure and the parallel current, along with the plasma boundary shape.

2. Dynamics of Turbulence Spreading

If turbulence can spread or propagate radially, the level of fluctuations at one radial place can depend on the drive of instabilities located elsewhere. This results in transport nonlocality. Indeed, a number of global transport phenomena can occur as a direct consequence of turbulence spreading. While turbulence spreading has been widely observed in direct numerical simulations since 1994[2], the recent high level of interest has revived as this has been identified as a physics mechanism[3] responsible for the deviation of transport scaling from gyroBohm scaling at moderate system sizes. A nonlocal mechanism is

necessary to explain this, since local turbulence characteristics compatible with gyroBohm scaling are observed in global nonlinear gyrokinetic simulations of ITG turbulence[4].

The role of turbulence spreading in breaking the gyroBohm scaling of transport has been further confirmed from a different gyrokinetic simulation [5] and from different theoretical considerations[6]. More recent applications of turbulence spreading include edge-core coupling[7], turbulence tunneling through a linearly stable gap[8], the role of zonal flows[9, 10], applications to reversed shear plasmas [11], the particle transport problem[12], and extensions to a multi-field model[10].

To enhance our understanding of physics mechanisms behind turbulence spreading, we performed a series of numerical experiments using the aforementioned new version of the GTC code. First, we examine the global turbulence evolution dynamics. An overall picture of global turbulence development due to turbulence spreading is illustrated in Fig. 1. This is from an ITG simulation for geometry and plasma parameters which are roughly based on DIII-D. The turbulence is driven by the ion temperature gradient which exceeds the linear threshold in the region $0.42 < r < 0.76$. As expected from previous simulations[13], finite amplitude turbulence spreads both inward and outward in the radial direction, into the linearly stable regions. The fluctuation intensity level in the linearly stable region is considerable compared to that in the original linearly unstable region. Figs. 1-a, b, and c are contour plots for three snapshots of the electric potential fluctuation on a poloidal plane, which illustrate the evolution of turbulence. At an early time (Fig. 1-a) before nonlinear saturation, radially elongated toroidal eigenmodes[14] are generated in the linearly unstable region with a small extension into the linearly stable zone via linear toroidal coupling. Later on, turbulence eddies are broken up by the self-generated $\mathbf{E} \times \mathbf{B}$ shear flows (zonal flows) during the nonlinear saturation phase. While the spreading is initiated as the toroidal eigenmodes are broken into smaller radial scale fluctuations by the zonal flows(Fig 1-b), most of turbulence spreading occur on a longer time scale after the local nonlinear saturation of turbulence (Fig 1-c). These fluctuations eventually evolve into a widely spread global turbulence envelope.

It is important to note that during turbulence spreading in our simulation, the profile relaxation is negligible. Therefore, the spreading is not a consequence of changes in the linear stability. Indeed, the $\mathbf{k}$-spectrum of fluctuations observed in the linearly stable region is significantly different from that of the ITG linear eigenmodes. The k_θ-spectra are significantly down-shifted relative to those of in the linearly unstable region.

As an example of mesoscale phenomena[15, 16] which occur on scales larger than an eddy size but smaller than the system size, turbulence spreading is quite a generic phenomenon as observed in global simulations in both toroidal geometry[17] and in the absence of toroidal coupling[18, 19], and both with[13] and without[20] zonal flows. To identify the relative roles of the linear toroidal mode coupling, nonlinear mode coupling, and self-generated zonal flows, we have carried out a series of numerical experiments to examine the properties of turbulence spreading associated with different mechanisms. In the absence of nonlinear mode coupling, as shown in Fig. 2-a, convective spreading occurs due the linear toroidal mode coupling in agreement with a previous theory prediction by Garbet[2]. The convective spreading observed in this linear simulation is characterized by a constant front propagation velocity $V_s \simeq (\rho_i/R)C_s$, which is also independent of the turbulence intensity.

As we turn on the nonlinearity, but with zonal flows artifically suppressed, the temporal

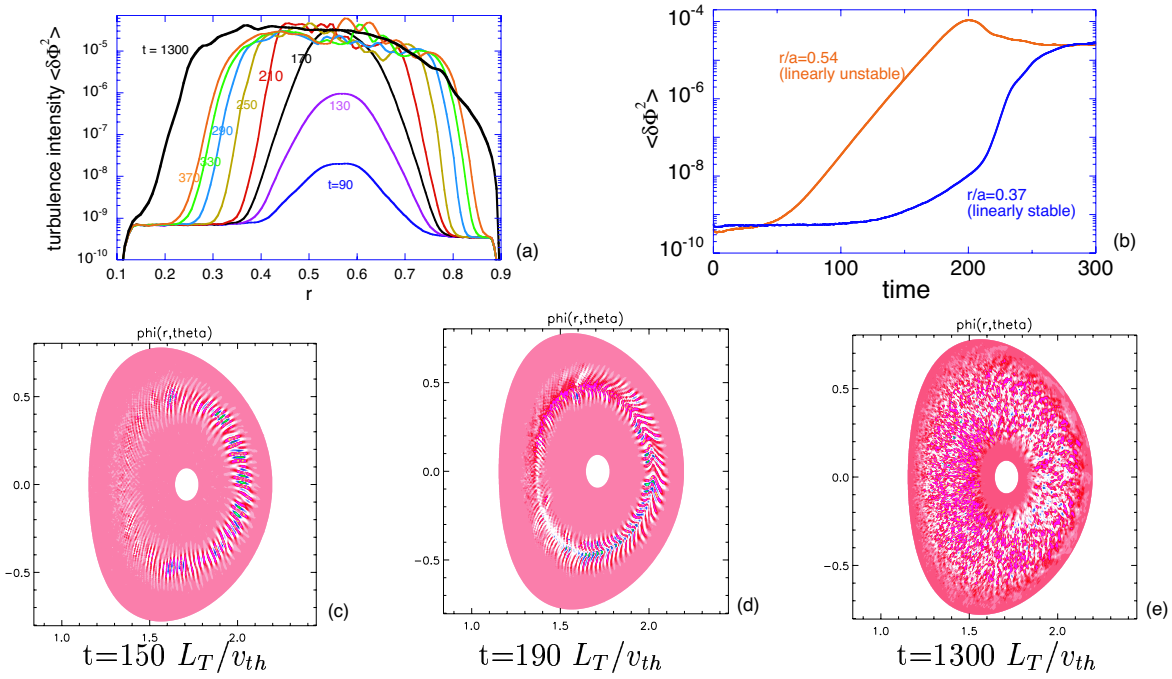

Figure 1: (a) Spatio-temporal evolution of flux surface averaged turbulence intensity, (b) time evolution of the intensity at two radii, and (c-e) contour plots for three snapshots of the electric potential on a poloidal plane, from a simulation of a shaped plasma with typical DIII-D parameters.

behavior of spreading becomes more complex. First, the turbulence spreading is much faster than that in the linear simulation. The front propagation velocity appears to be "convective" in the linearly unstable zone in agreement with the Fisher-Kolmogorov solution[8]. As the front approaches the region of weaker linear drive, it slows down and the propagation can be described as "diffusive" or "sub-diffusive"[3]. The turbulence spreading finally stops when the front reaches the region of strong linear damping.

Finally, the fluctuation envelope evolution, from simulations with the self-generated zonal flows, is plotted in Fig 1-a. The principle effect of zonal flows is to reduce the intensity of fluctuations, approximately by a factor of 10. Consequently, the spreading velocity is reduced as well. It is important to note that while zonal flows play a crucial role in determining the saturation value of the fluctuation intensity, there are many other channels of nonlinear mode coupling which can saturate fluctuations even in the absence of zonal flows. Therefore, it is hard to isolate the possible role of zonal flows in enhancing turbulence spreading, which has been predicted from an extension of the 4-wave theory[6, 9] in which only the zonal flow mediated nonlinear interaction is kept. At least for the cases we have simulated, zonal flow induced enhancement of turbulence spreading has not been observed. A related theoretical discussion can be found in Gurcan et al.[10].

To elaborate our description of turbulence spreading dynamics in a more quantitative fashion, we perform the following analysis of the simulation data. We measure the turbulence propagation velocity at each radius by recording the time at which the fluctuation front of a specified turbulence intensity passes through that point. Using the turbulence

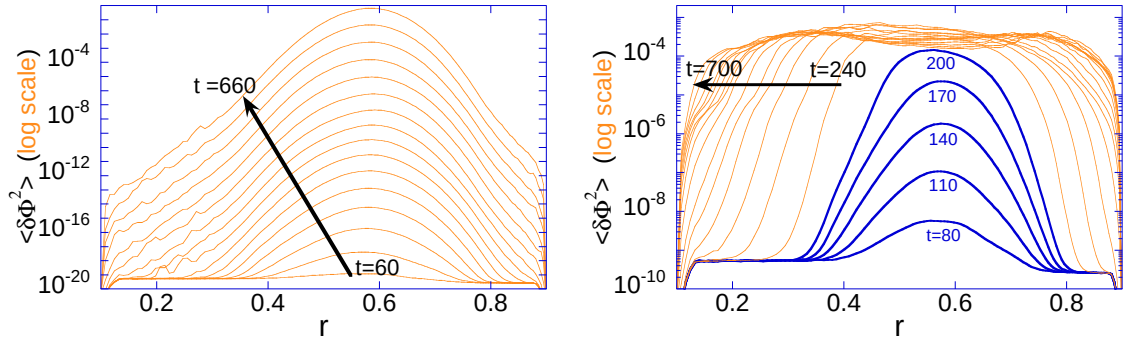

Figure 2: Spatio-temporal evolution of turbulence intensity: (left) linear simulation with all modes and (right) nonlinear simulation without zonal flows.

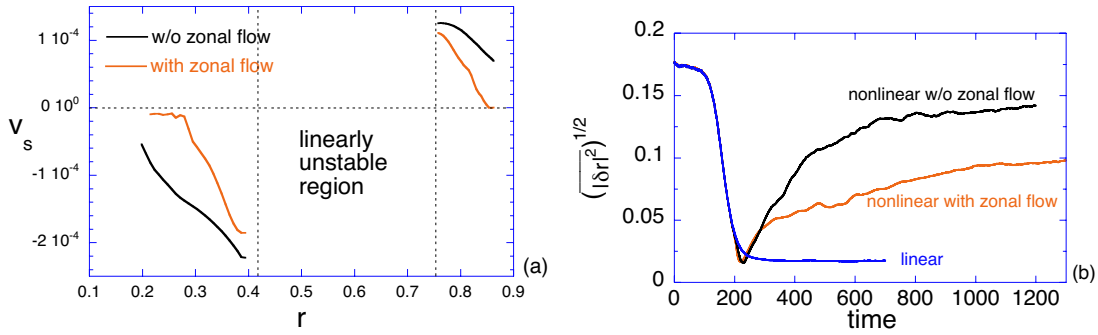

Figure 3: (a) Turbulence propagation velocity (positive and negative velocities indicate outward and inward propagation respectively.) (b) Intensity weighted displacement of turbulence fluctuations vs time during turbulence spreading.

intensity, $< \delta\Phi^2 >= 10^{-6}$, we have obtained the results shown in Fig. 3-a. After recording the arrival time of the turbulence propagation front as a function of radius, we obtained the turbulence propagation velocity plotted in Fig. 3-a. It is observed that the turbulence propagation becomes slower as fluctuations propagate away from the linearly unstable region. In addition, in the presence of self-generated zonal flows, the propagation velocity is significantly reduced.

Next, we define the radial extent of the fluctuation envelope using the following expression,

$$\overline{|\Delta r|^2} \equiv \frac{\int_{r_1}^{r_c} d^3x (r - r_c)^2 |\delta\phi|^2}{\int_{r_1}^{r_c} d^3x |\delta\phi|^2},$$

where the spatial integral is performed over the linearly stable region from the inner boundary of the simulation domain ($r_1 = 0.1$ for this simulation) to the point where the linear growth rate vanishes ($r_c = 0.42$). The resulting displacement $(\overline{|\Delta r|^2})^{1/2}$ is also a quantitative measure of turbulence spreading. The time evolution of $(\overline{|\Delta r|^2})^{1/2}$ is plotted in Fig. 3-b. It clearly illustrates that most of the turbulence spreading starts at about $t = 200$, right after the local nonlinear saturation of the ITG instability. Both simulations with and without zonal flows show a gradual transition from convective to diffusive (and possibly sub-diffusive) propagation. The spreading is reduced in the presence of zonal

flows, as discussed before. Finally, we note that the initial high level of $(\overline{|\Delta r|^2})^{1/2}$ is due to the spatially-uniform initial loading of small random fluctuations which are not turbulence generated by plasmas. Therefore, only the evolution after $t = 200$ makes physical sense.

3. Turbulence spreading through a transport barrier: the role of $\mathbf{E} \times \mathbf{B}$ flow shear

Sometimes, nonzero turbulence levels and anomalous transport are observed in a region where there is no instability drive. For instance, in JT-60U reversed shear plasmas, reflectometry measurements clearly show the existence of turbulence in the region where profiles are flat, and the microinstabilities are stable[21]. Therefore, we are faced with the following natural question: "Can turbulence spread through a transport barrier?" To address this problem, we performed a number of numerical experiments using the new version of the GTC code with shaping, by placing an $\mathbf{E} \times \mathbf{B}$ shear layer, with varying depths of the E_r well, next to the linearly unstable zone, as shown in Fig. 4-a.

From the simulations, we observe that the extent of the turbulence spreading decreases with increasing $\mathbf{E} \times \mathbf{B}$ shear. From the simulations, we observe that the extent of the turbulence spreading is significantly reduced as the E_r well gets deeper (Fig. 4-a). We also observe that the spreading speed is controlled by the local value of the $\mathbf{E} \times \mathbf{B}$ shearing rate[22]. As one can see from Fig. 4-b, the fluctuation front propagation slows down significantly when it crosses regions of the local maximum of the $\mathbf{E} \times \mathbf{B}$ shearing rate. The overall spatio-temporal evolution of front propagation is consistent with the fact that the front propagation speed increases with the fluctuation intensity, and the fact that the $\mathbf{E} \times \mathbf{B}$ shear (not E_r) reduces the fluctuation intensity locally.

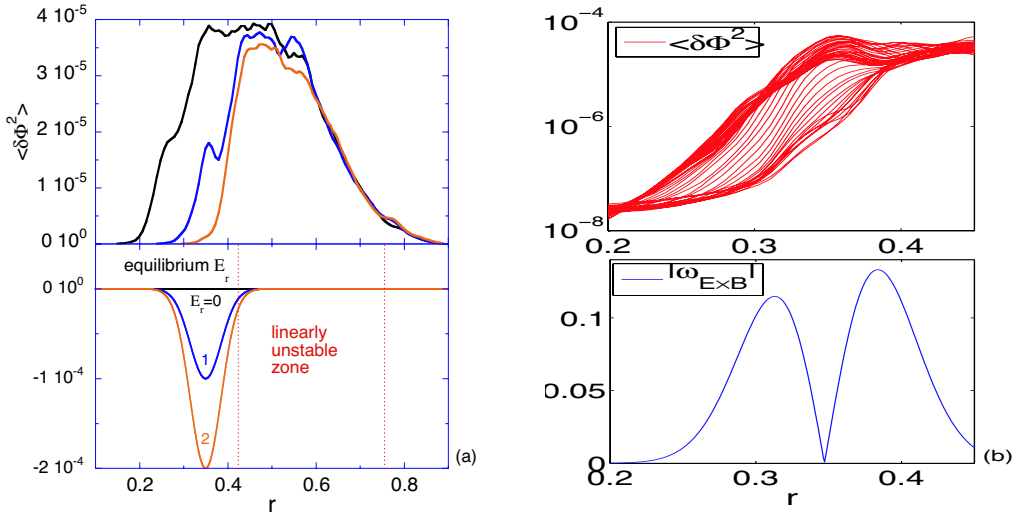

Figure 4: (a) The radial extent of turbulence spreading (of steady state fluctuation intensity) is reduced, as the $\mathbf{E} \times \mathbf{B}$ shear layer, located next to the unstable ITG source region, becomes deeper, with corresponding $\omega_{E\times B} = 0.13 C_s/a$, and $\omega_{E\times B} = 0.26 C_s/a$, respectively. (b) The spatio-temporal evolution of the propagation front shows that the spreading slows down significantly at the local maxima of the $\mathbf{E} \times \mathbf{B}$ shearing rate.

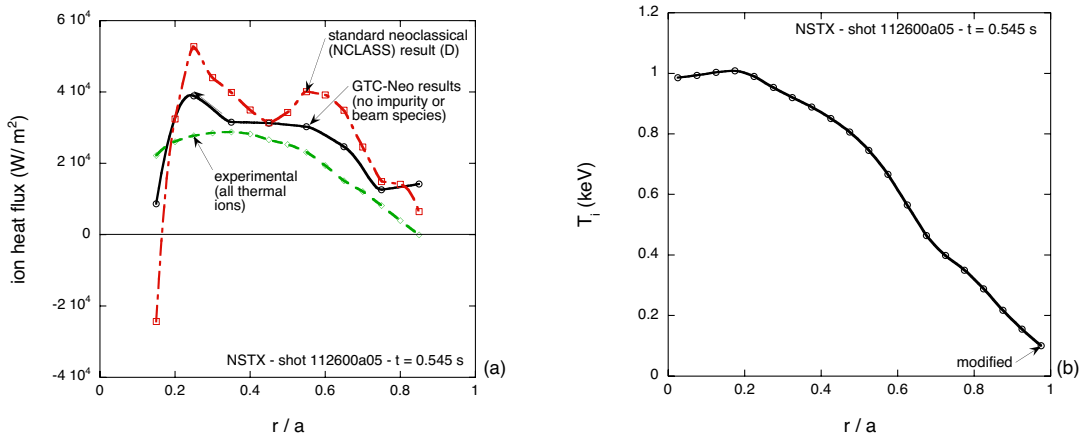

Figure 5: (a) Simulated neoclassical ion heat flux of an NSTX plasma, compared with the experimental measurement and the prediction of standard neoclassical theory. (b) Ion temperature profile of NSTX plasma used in simulation.

Based on our previous theory[3], the nonlinear diffusion will cause a front to propagate in radius. In the absence of dissipation, the front will propagate indefinitely with its shape being maintained. The front propagation stops when the radial flux due to propagation is balanced by dissipation. We can estimate the extent of turbulence spreading into the linearly stable zone by equating the time required for the front to propagate a distance Δ to the inverse of the linear damping rate, which increases with radius.

We have obtained a simple formula which shows that the extent of spreading increases with the intensity and decreases with the linear damping rate, *i.e.*, $\Delta \propto \sqrt{V_s/|\gamma|'}$. Therefore, the results depend on the profiles used. One can extend the previous calculation by including the damping from the $\mathbf{E} \times \mathbf{B}$ shearing rate, and we can get a rough prediction of the turbulence spreading extent as a function of the $\mathbf{E} \times \mathbf{B}$ shearing rate profile from the same procedure.

4. Nonlocal neoclassical transport

For neoclassical transport, the nonlocality is caused by ion drift orbits whose width can be larger than the local minor radius and/or the plasma equilibrium scale length. Our global neoclassical particle simulation using GTC-Neo[23], which includes nonlocal physics due to large orbit effects, studies neoclassical physics of NSTX plasmas. It is observed that neoclassical transport in NSTX plasmas exhibits a nonlocal nature. Typically, near the magnetic axis, the ion heat flux is decoupled from the local temperature gradient, breaking the Fick's law type gradient-flux relation. As shown in Fig. 5, our simulation predicts an outward ion heat flux, even for a reversed local ∇T_i near the magnetic axis, which is in the same direction as the experimental measurement. For a wide range of NSTX shots, nonlocal effects generally bring the simulated ion heat transport into closer agreement with the experimental measurements. Our neoclassical simulation is also being extended to anisotropic plasmas with large flows, a theoretically unexplored experimental condition, for a better understanding of large poloidal flows observed in DIII-D experiments[24].

Acknowledgments

We acknowledge useful interactions with P.H. Diamond, X. Garbet, Ph. Ghendrih, O. Gurcan, F.L. Hinton, Y. Idomura, K. Itoh, S.-I. Itoh, Z. Lin, V. Naulin, L. Villard, M. Yagi, and F. Zonca. This work was supported by U.S. DoE Contract No. DE-AC02-76-CHO-3073 and in part by the U.S. DoE SciDAC Center for Gyrokinetic Particle Simulation of Turbulent Transport in Burning Plasmas.

References

[1] W. X. Wang, Z. Lin, W. M. Tang *et al.*, Phys. Plasmas **13**, 092505 (2006).

[2] X. Garbet, L. Laurent, A. Samain, and J. Chinardet, Nucl. Fusion **34**, 963 (1994).

[3] T. S. Hahm, P.H. Diamond, Z. Lin *et al.*, Plasma Phys. Control. Fusion **46**, A323 (2004).

[4] Z. Lin, S. Ethier, T.S. Hahm *et al.,* Phys. Rev. Lett. **88**, 195004 (2002).

[5] R. E. Waltz and J. Candy, Phys. Plasmas **12**, 072303 (2005).

[6] L. Chen, R.B. White, F. Zonca, Phys. Rev. Lett. **92**, 075004 (2004).

[7] T. S. Hahm, P.H. Diamond, Z. Lin *et al.*, Phys. Plasmas **12**, 090903 (2005).

[8] O.D. Gurcan, P.H. Diamond, T.S. Hahm *et al.*, Phys. Plasmas **12**, 032303 (2005).

[9] F. Zonca, L. Chen, and R.B. White, *Theory of Fusion Plasmas*, (Proc. Joint Varenna-Lausanne Int. Workshop, Varenna, 2004) (Bologna: SIF) 3.

[10] O.D. Gurcan, P.H. Diamond, T.S. Hahm *et al.*, Phys. Plasmas **13**, 052306 (2006).

[11] M. Yagi, T. Ueda, S.-I. Itoh, *et al.*, Plasma Phys. Control. Fusion **48**, A409 (2006).

[12] V. Naulin *et al.,* Phys. Plasmas **12**, 122306 (2005).

[13] Z. Lin and T. S. Hahm, Phys. Plasmas **11**, 1099 (2004).

[14] W. Horton, D.-I. Choi, and W.M. Tang, Phys. Fluids **24**, 1077 (1981).

[15] P. H. Diamond and T. S. Hahm, Phys. Plasmas **2**, 3640 (1995).

[16] S.-I. Itoh and K. Itoh, Plasma Phys. Control. Fusion, **43**, 1055 (2000).

[17] R.D. Sydora *et al.*, Plasma Phys. Control. Fusion **38**, A281 (1996).

[18] Y. Idomura, M. Wakatani, and S. Tokuda, Phys. Plasmas **7**, 3551 (2000).

[19] L. Villard, S. J. Allfrey, A. Bottino *et al.*, Nucl. Fusion **44**, 172 (2004).

[20] S.E. Parker *et al.,* Phys. Plasmas **3**, 1959 (1996).

[21] R. Nazikian, K. Shinohara, G. J. Kramer *et al.*, Phys. Rev. Lett. **94**, 135002 (2005).

[22] T. S. Hahm and K. H. Burrell, Phys. Plasmas **2**, 1648 (1995).

[23] W. X. Wang, W. M. Tang, F. L. Hinton *et al.*, Computer Phys. Communications **164**, 178 (2004).

[24] W. M. Solomon, K. H. Burrell, R. Andre *et al.*, Phys. Plasmas **13**, 056116 (2006).